Preparation and Characterization of Polypropylene–Montmorillonite Nanocomposites Generated by *In Situ* Metallocene Catalyst Polymerization

Jyh-Ming Hwu,[1] George-J Jiang[2]

[1]*Union Chemical Laboratories, Industrial Technology Research Institute, Hsinchu, 300, Taiwan*
[2]*Department of Chemistry, Chung Yuan Christian University, Chungli, 320, Taiwan*

Received 8 June 2004; accepted 16 August 2004
DOI 10.1002/app.21325
Published online 19 January 2005 in Wiley InterScience (www.interscience.wiley.com).

ABSTRACT: An ion-exchange method was applied to replace sodium cations inside the interlamellar space of montmorillonite with positively charged stearyl trimethyl ammonium chloride. The d_{001}-spacing of montmorillonite is larger in toluene than in other solvents. The overexchanged stearyl methyl ammonium chloride in the montmorillonite layers can be completely washed out by ethanol. Polypropylene–montmorillonite nanocomposites were prepared by using the supported *rac*-Et(Ind)$_2$ZrCl$_2$ catalyst on the montmorillonite. The nanocomposites that were polymerized by the supported catalyst were characterized by infrared spectroscopy, nuclear magnetic resonance, X-ray diffraction, differential scanning calorimetry, scanning electron microscopy, and transmission electron microscopy. Transmission electron microcopy shows that each silicate sheet of montmorillonite is randomly dispersed into the polypropylene matrix following polymerization by using a supported catalyst. The polypropylene nanocomposites had higher crystallinity, hardness, and thermal properties than pure polypropylene. © 2005 Wiley Periodicals, Inc. J Appl Polym Sci 95: 1228–1236, 2005

Key words: polypropylene; nanocomposites; *in situ* polymerization

INTRODUCTION

Polymer composites have been extensively used in various areas, including electronics, transportation, construction, and consumer products. They provide several benefits, the most important of which includes unusual combinations of stiffness and toughness, which are difficult to derive from the individual components. Recently, families of nanocomposites have received increasing attention. A nanocomposite is defined as a composite characterized by particles with an observed dispersed phase of $<$100 nm. This nanometer size effect generally corresponds to very large relative surface areas and strong interactions with the polymer matrix, causing nanocomposites to exhibit unique characteristics that are not typically shared by their more conventional composite counterparts. Therefore, nanocomposites provide new technology and business opportunities.

For example, montmorillonite (Mont) is a clay mineral that consists of stacked silicate sheets with a thickness of $\sim$1.00 nm. It undergoes intercalation with various organic molecules. Through such intercalation, several useful polymer–clay nanocomposites have been produced, including nylon–clay hybrid,[1,2] polystyrene–clay hybrid,[3–5] polyimide–clay hybrid,[6] poly(methyl methacrylate)–clay hybrid,[7–9] and polypropylene–clay hybrid.[10–13] Each of these nanocomposites has a particular use. However, dispersing silicate layers of Mont at the nanometer level in nonpolar polymers is difficult.

The appearance of coordinated catalytic polymerization has led to the support of a new generation catalyst on organic or inorganic materials.[14] The first supported organometallic catalyst was prepared by depositing chromium hexacarbonyl and molybdenum over Al_2O_3.[15,16] Catalysts that contain molybdenum were used in the metathesis of olefins; however, chromium-containing catalysts were active in ethylene polymerization.

Metallocene catalysts activated by methylaluminoxane (MAO) exhibit strong activity in olefin polymerization reactions.[17,18] The extensively studied characteristics of polymers, such as thermal resistance, hardness, impact strength, and transparency, can be precisely controlled through the metallocene structure. Metallocene catalyst systems have been used to polymerize ethylene,[19,20] propylene,[21] and methyl methacrylate monomers.[22] Remarkably, the use of immobilized metallocene catalysts results in the formation of uniform polymer particles with a narrower size distribution and higher bulk density than those provided by metallocene immobilized catalysts.[23] Meth-

Correspondence to: J.-M. Hwu (ryanhu@itri.org.tw).

ods for immobilizing metallocene fall into two broad categories: (1) MAO-mediated systems, in which the impregnation of the support with MAO is followed by the addition of metallocene[24,25]; and (2) directly impregnated systems, in which the modification of the support with MAO is immobilized.[26,27] The procedures generate different catalysts, which yield polyolefins with different characteristics.

Recently, Tudor et al. demonstrated the ability of soluble metallocene catalysts to intercalate inside silicate layers and promote the coordination polymerization of propylene.[28] Hectorite was first treated with MAO to remove all acidic protons and to prepare the interlayer spacing to obtain the catalyst. Upon the addition of the metallocene catalyst, a cation exchange occurred with sodium cations and the catalyst was incorporated in the hectorite galleries. This metallocene-immobilized catalyst exhibited high activity in the polymerization of propylene when in contact with an excess of MAO, producing polypropylene (PP) oligomers. Unfortunately, this method did not characterize the composite.

In this study, the polypropylene–montmorillonite (PP-Mont) nanocomposites were prepared by *rac*-Et(Ind)$_2$ZrCl$_2$ catalyst supported on montmorillonite. PP is one of the most extensively used polymers as it has a relatively uniform composition and participates predictably in reactions. It has no polar groups in its backbone so the well-dispersion of the silicate layers in PP cannot be realized. An *in situ* method was used to prepare PP-Mont nanocomposites by selecting stearyl trimethyl ammonium chloride (SAC) to increase the d_{001}-spacing of Mont. SAC can increase the interlayer distance of Mont; then the catalyst can be supported on the montmorillonite. The propagation of PP polymerization can increase the interlayer distance of montmorillonite and is dispersed randomly. This synthesis of the nanocomposite reveals the improved thermal, mechanical, and barrier characteristics, in comparison with those of pure PP. The structure and some of the characteristics of such composites will be considered.

EXPERIMENTAL

Materials

The clay materials used in synthesizing PP-Mont nanocomposites are the sodium-type montmorillonite (CEC = 1.15 meq/g). The swelling agent of SAC was obtained from Akzo Nobel Chemical Inc. The *rac*-Et(Ind)$_2$ZrCl$_2$ catalyst and MAO cocatalyst were obtained from Aldrich Co., Ltd. The propylene gas was purchased from Jian Reeng Gases Co. (Chungli, Taiwan). Toluene was dried over sodium lumps and distilled before use.

Preparation of organomontmorillonite

In 600 mL of solvent, 10 g sodium montmorillonite was added to a solution of SAC and concentrated orthophosphoric acid (0.5 mL). The mixture was stirred vigorously at 80°C for 24 h. (When acetone was used as a solvent, the reaction temperature was 30°C.) A white precipitate was isolated by filtration and then washed five times with the reaction solvent. The organomontmorillonite (O-Mont) was then collected after it was dried in a vacuum for 8 h.

Preparation of *rac*-Et(Ind)$_2$ZrCl$_2$ supported catalyst

The organomontmorillonite was suspended in the MAO solution (5 mmol in toluene) and reacted at room temperature for 1 h. It was filtered in a Schlenk apparatus and washed four times with toluene until the washing solution was observed to be clear, $\sim$ 80 wt % aluminum on the montmorillonite. It was then added to 5 mL toluene that contained 5 μmol of *rac*-Et(Ind)$_2$ZrCl$_2$; it was stirred for 1 h at room temperature, washed four times with toluene, and dried under vacuum. The *rac*-Et(Ind)$_2$ZrCl$_2$ catalysts were successfully supported on the montmorillonite.

Preparation of PP-Mont nanocomposites

PP-Mont nanocomposites were polymerized from PP by using the *rac*-Et(Ind)$_2$ZrCl$_2$-supported catalyst. Toluene (100 mL) was added to a Parr reactor under an atmosphere of nitrogen. After a fixed reaction temperature was obtained (the reaction conditions are shown in Table II), the supported catalysts were added to catalyze the polymerization. After 1 h of polymerization, 5 mL dilute solution of HCl in methanol was added to terminate the polymerization. The products were isolated by filtration and washed with methanol before they were dried under a vacuum.

Characterization

X-ray diffraction (XRD) measurements were taken by using CuKα radiation, at 30 kV and 20 mA. The nuclear magnetic resonance (NMR) spectrum was obtained in 1,1,2,2-tetrachloroethane-d_2 at 80°C by using a Cuchi Re-300 NMR spectrometer. The Fourier transform infrared (FTIR) spectrum was measured by using Bio-Rad FTS-7 cast on KBr. The melt temperature (T_m) and enthalpy (ΔH) were measured by using a Seiko DSC-200 calorimeter at a heating rate of 10°C/min. The decomposition temperature (T_d) was measured by using a TA2950 thermal gravimetric analyzer (TGA), at a heating rate of 5°C/min to 600°C in an environment of nitrogen. A transmission electron micrograph (TEM) was obtained by using a JEM-1200 EXII (JEOL) at an acceleration voltage of 120 kV. The scanning

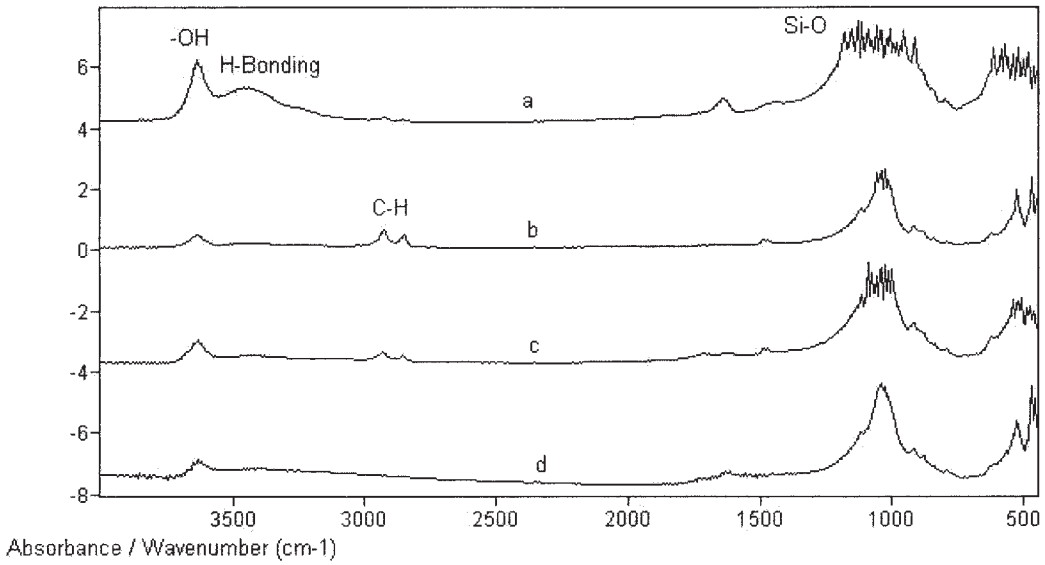

Figure 1 The FTIR spectrum of (a) sodium-Mont; (b) O-Mont (prepared by SAC); (c) O-Mont heated to 300°C; (d) O-Mont heated to 500°C.

electron micrograph (SEM) image of gold-coated polymer powders was recorded by using a JSM-6300 (JEOL) at an accelerating voltage of 20 kV. The bulk density was obtained from a Mirage, MD-200S, and the hardness was measured by using an Akashi micro-Vickers hardness testing machine, MVK-H0, with a test force of 0.98 N.

RESULTS AND DISCUSSION

Characteristics of organomontmorillonite

SAC was used as the swelling agent for Mont. Figure 1(a, b) presents the FTIR absorption bands of sodium-Mont and SAC-Mont (the sodium montmorillonite was modified by SAC). The absorption at 3650 cm^{-1} is attributed to the O—H vibration; absorption at 3200 cm^{-1} is due to the intermolecular hydrogen bond between the stacked silicate sheets, and absorption at 1030 cm^{-1} is associated with Si—O stretching. The absorption of the intermolecular hydrogen bond declines after the sodium-Mont was ion-exchanged with SAC [Fig. 1(b)] because the layer spacing of Mont is increased. The organic C—H vibrations of SAC are therefore at 2850 and 2900 cm^{-1}.

Table I presents the XRD results. Bragg's law ($n\lambda = 2d \sin \theta$, d = layer distances) determines the distances between the silicate layers. The wavelength (λ) of CuKα X-rays is 0.15418 nm. The measured d_{001}-spacing of pristine montmorillonite is 1.4 nm ($2\theta = 6.25°$). The O-Mont exchanged using toluene as the solvent has the greatest d_{001}-spacing ($2\theta = 3.9°$, $d_{001} = 2.26$ nm). However, the XRD result still has pristine montmorillonite peaks at 6.25° and 7.10°, which is due to the nonreactive sodium-Mont still present in O-Mont exchanged in toluene. On the other hand, ethanol is a very good solvent that can wash out the overexchanged swelling agents (Fig. 2). The d_{001}-spacing of O-Mont only increases 0.1 nm after swelling by SAC in ethanol.

A higher temperature is required when preparing polymer–clay nanocomposites by using either *in situ* polymerization or melt intercalation. However, if the temperature at which polymer–clay nanocomposites are synthesized exceeds the thermal stability of the organoclay, then decomposition will take place. The temperature of the onset of decomposition of organoclay is therefore important in making polymer–clay nanocomposites. The degradation is very sensitive to the quantity of the organic interface in the layered silicate, so understanding the upper processing temperature and the environment of these nanocomposites is very important. Four different solvents for ion-exchange with an SAC swelling agent, including deionized water, acetone, ethanol, and toluene, were used to understand how the ion-exchange environment influences the thermal stability and the structure of O-Mont.

Figure 3 plots derivative thermogravimetric analysis (DTG) curves of O-Mont prepared in various solvents. The evolution of water from sodium Mont is considered across two regions of the curve.[29] The regions of free water and interlayer water evolution are in the temperature range 40–300°C, and the region of structural water evolution is in the temperature range 500-1000°C, over which the bonded OH group undergoes dehydroxylation. However, the DTG curves of O-Mont, plotted in Figure 3, are more conveniently considered as four regions under the experimental

TABLE I
Properties of O-Mont Prepared in Different Solvents[a]

No.	Solvent (600 ml)	$2\theta_{max}$ (degree)	d_{001}-spacing (nm)	T_1[b] (°C)	T_2[c] (°C)	Residue[d] (wt %)
Na-1	—	6.25	1.41	—	—	90.9
Sa-1	DI-water	4.80	1.84	164.8	312.3	74.2
Sa-2	Acetone	4.95	1.78	188.8	307.6	77.0
Sa-3	Ethanol	5.90	1.50	229.8	—	81.3
Sa-4	Toluene	3.90	2.26	256.4	354.4	72.8

[a] Sodium mont = 10 g (CEC = 1.15 meq/g), reaction time = 24 h, reaction temperature = 80°C (acetone at 30°C).
[b] T_1 = first onset decomposition temperature of swelling agent.
[c] T_2 = second onset decomposition temperature of swelling agent.
[d] Residue weight percent at 1000°C.

conditions used herein. The free water region is at temperatures < 200°C. The region in which organic substances evolved was in the temperature range from 200 to 500°C. The structural water region is in the temperature range from 500 to 800°C. Between 800 and 1000°C, carbon reacts in some yet unknown way. The release of organic species from O-Mont is a two-step process, associated with the presence of the organic modifier, the overexchanged organic modifiers, and bonded organic modifiers among the Mont layers (see Fig. 2). As revealed by the DTG curve of O-Mont samples, the derivative weight loss reaches a steady-state plateau before the first DTG peak. Hence, the temperature at which the derivatives weight loss is 0.001%/°C over the value at the plateau denoted as the temperature (T_1) of the first onset of decomposition. The temperature at which the derivative weight loss between the first and second weight loss peaks is lowest as the second temperature (T_2) of the onset of decomposition. Table I summarizes the results. For the O-Mont prepared in the deionized water, the first onset decomposition temperature is 164°C, which is similar to that of the swelling agent SAC. For the O-Mont prepared in toluene, ~ 5% weight is lost in the temperature from 110 to 210°C. The aromatic solvent toluene can penetrate the Mont layer and remain there even after drying. The O-Mont prepared in toluene has the highest T_1 and T_2 (T_1 = 256.4°C, T_2 = 354.4°C), because the organic modifier can enter the Mont layers completely. When ethanol is used as the solvent, only one organic decomposition peak is evident between 200 and 400°C, since the overexchanged organic modifiers can be dissolved and washed out by ethanol. Therefore, only bonded organic modifiers are present in ethanol-prepared organomontmorillonite. The details of the decomposition mechanism of the decomposition of organic modified montmorillonite have been discussed elsewhere (similar to Fig. 4).[30] The water detected at 110°C may be absorbed water. At higher temperatures, the water is produced by the reaction of the hydroxyl group in the montmorillonite sheets with organic modifiers. The bond between N and C in the organic modifiers outside the montmorillonite sheets may break first at around 200°C. The montmorillonite sheets exhibit less hindrance and so can evolve quickly without further degradation. At higher temperatures, organic treatments decompose from the montmorillonite sheets. The hindrance in the montmorillonite sheets and the force between these sheets are such that the sheets evolve slowly, and further decomposition occurs mainly between C and C bonds.

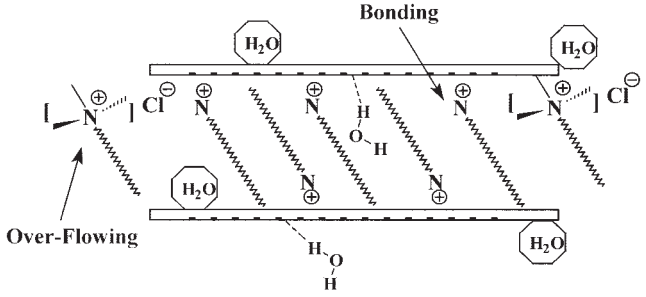

Figure 2 The situation of O-Mont prepared by ammonium swelling agent.

Sample Sa-1 was heated from room temperature to 300 and 500°C and then examined by both FTIR and XRD to verify that an organic substance is decomposed over the temperature range 200–500°C. For comparison, FTIR and XRD experiments on the unheated Sa-1 and sodium-Mont are also conducted. Figure 1 indicates clearly that organic C—H vibrations (2853 and 2629 cm^{-1}) decline after the Sa-1 sample was pyrolyzed to 300°C [Fig. 1(c)]. When the Sa-1 sample was heated to 500°C, the C—H vibration completely disappeared [Fig. 1(d)]. Meanwhile, the OH absorption (wavenumber = 3690, 3620, and 1636 cm^{-1}) of pyrolyzed samples does not change in either frequency or intensity. Hence, most weight losses over the temperature range from 200 to 500°C are due to the decomposition of organic compounds. Figure 5

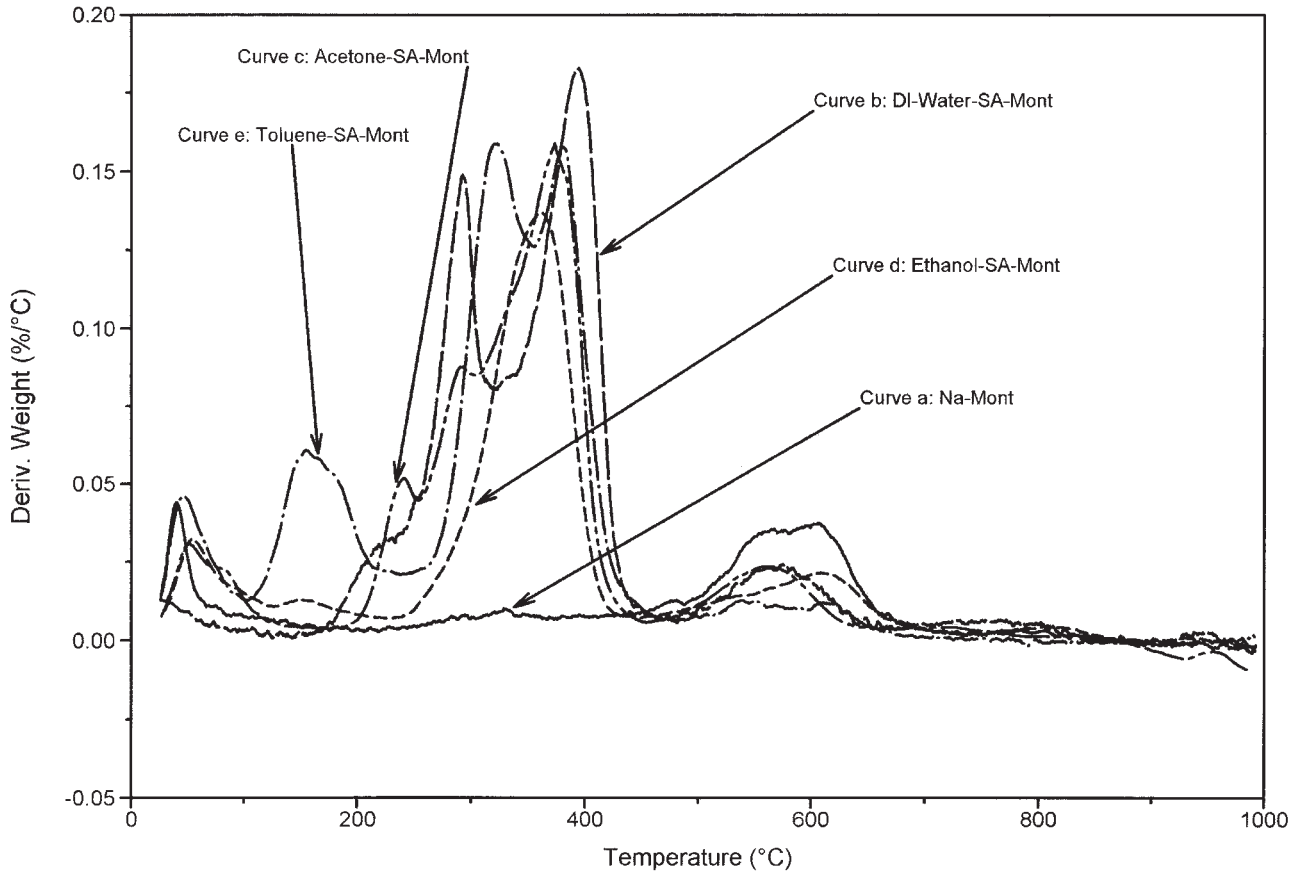

Figure 3 The HDTG curves of (a) sodium-Mont and O-Mont prepared in (b) deionized water; (c) acetone; (d) ethanol; (e) toluene.

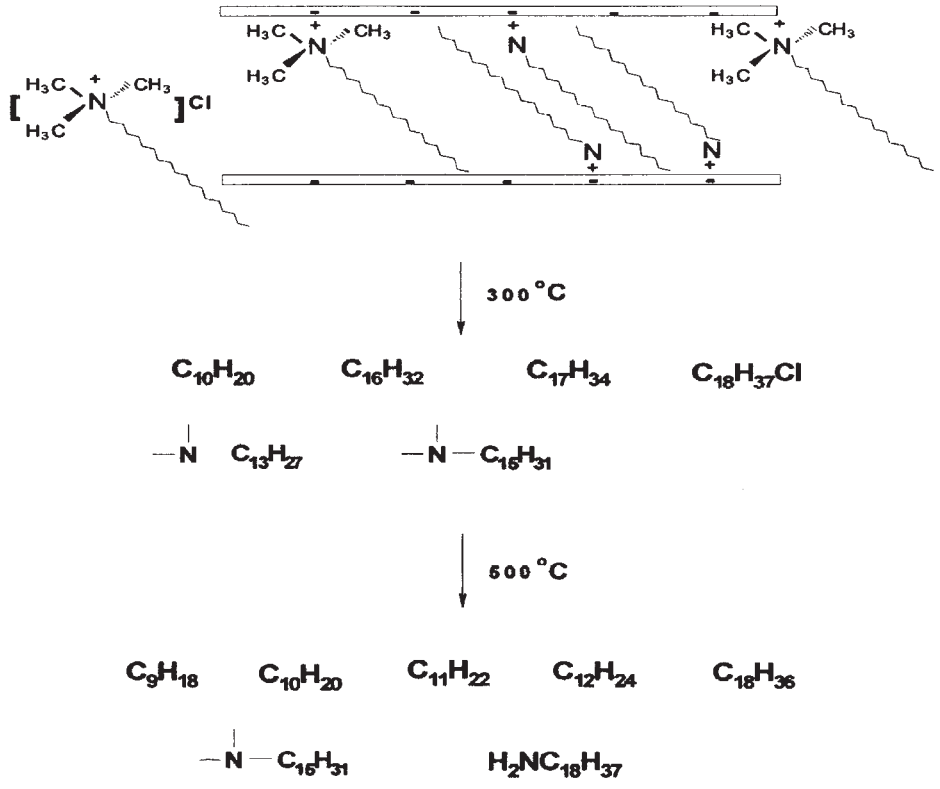

Figure 4 The probable decomposition mechanism of O-Mont prepared by SAC.

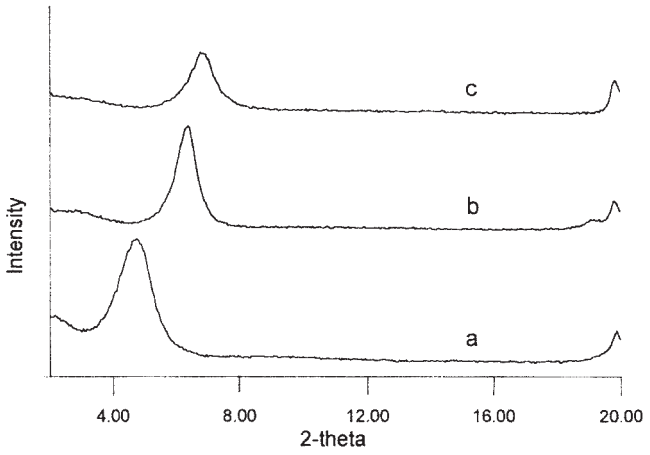

Figure 5 The XRD patterns of (a) O-Mont (prepared by SAC); (b) O-Mont heated to 300°C; (c) O-Mont heated to 500°C.

presents XRD results that confirm the foregoing observation. After sample Sa-1 was heated to 300°C for 1 h, its d_{001}-spacing fell to 1.4 nm [from Fig. 5(a, b)]; after it was heat-treated at 500°C, all the organic modifiers were decomposed and the layer distances were restored to those of pristine sodium-Mont [Fig. 5(c)].

Characteristics of PP-Mont nanocomposites

Metallocene catalysts cannot be used in polymerizing polar functional monomers because the polar functional group mitigates the activity of metallocene catalysts. Scientists who have sought to polymerize propylene directly in the layers of Mont have found that functional groups such as hydroxyl groups and silicon dioxide groups poison the metallocene catalyst. The metallocene-supported catalysts on the silicon dioxide group of Mont were prepared to polymerize propylene to solve this problem (Fig. 6). When the montmorillonite was treated with MAO, a chemical reaction between the hydroxyl group and alkylaluminum compounds occurred (compound I). Upon further introduction of zirconocene, an anchoring is observed on the supporting surface via an interaction with compound I to form the supported catalyst from compound II. The FTIR spectrum in Figure 7 indicates the structure of PP and PP-Mont nanocomposites from the supported catalyst of compound II. The peak at 2800–2900 cm^{-1} is associated with C—H stretching; those at 1390 and 1450 cm^{-1} are attributed to C—H bending. The PP-Mont retains the OH group with absorption at 3650 cm^{-1} and the Si—O group with absorption at 1030 cm^{-1} from the pristine montmorillonite.

Figure 8 presents XRD patterns of PP and PP-Mont. Pure PP yields three peaks at 14, 16.8, and 18.6° because of different crystalline domains are present in the construction. When the supported catalyst is used to obtain the PP-Mont nanocomposite, the O-Mont peak at 4.8° disappears, and the PP peaks remains. The results clearly reveal that the layers of Mont have been broken. Restated, the silicate sheets of Mont in the PP matrix are completely dispersed. A TEM picture of PP-Mont nanocomposites verified the foregoing observation in Figure 9. The dark lines represent intersections among silicate sheets of Mont and each silicate sheet of Mont is randomly dispersed into the PP matrix following polymerization by using a supported catalyst.

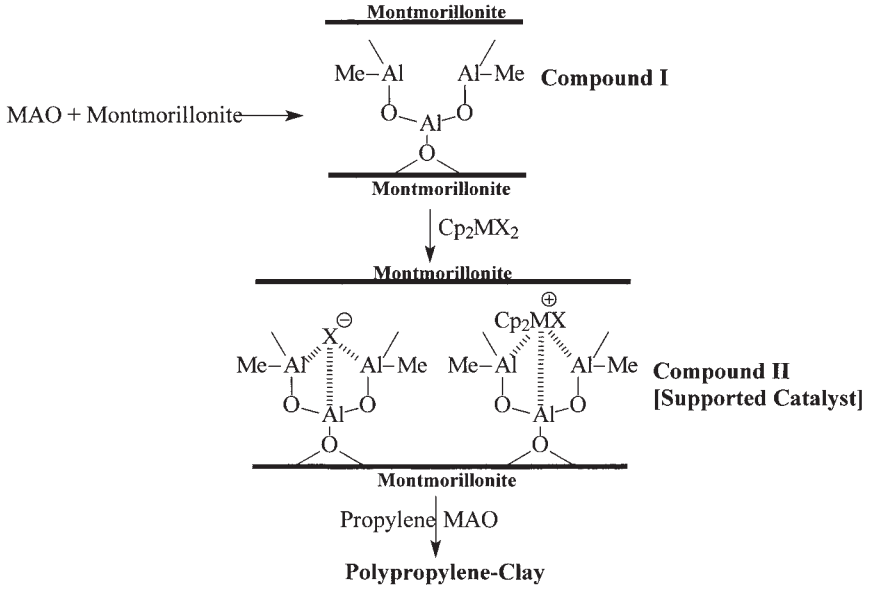

Figure 6 The synthesis mechanism of *rac*-Et$(Ind)_2ZrCl_2$-supported catalyst.

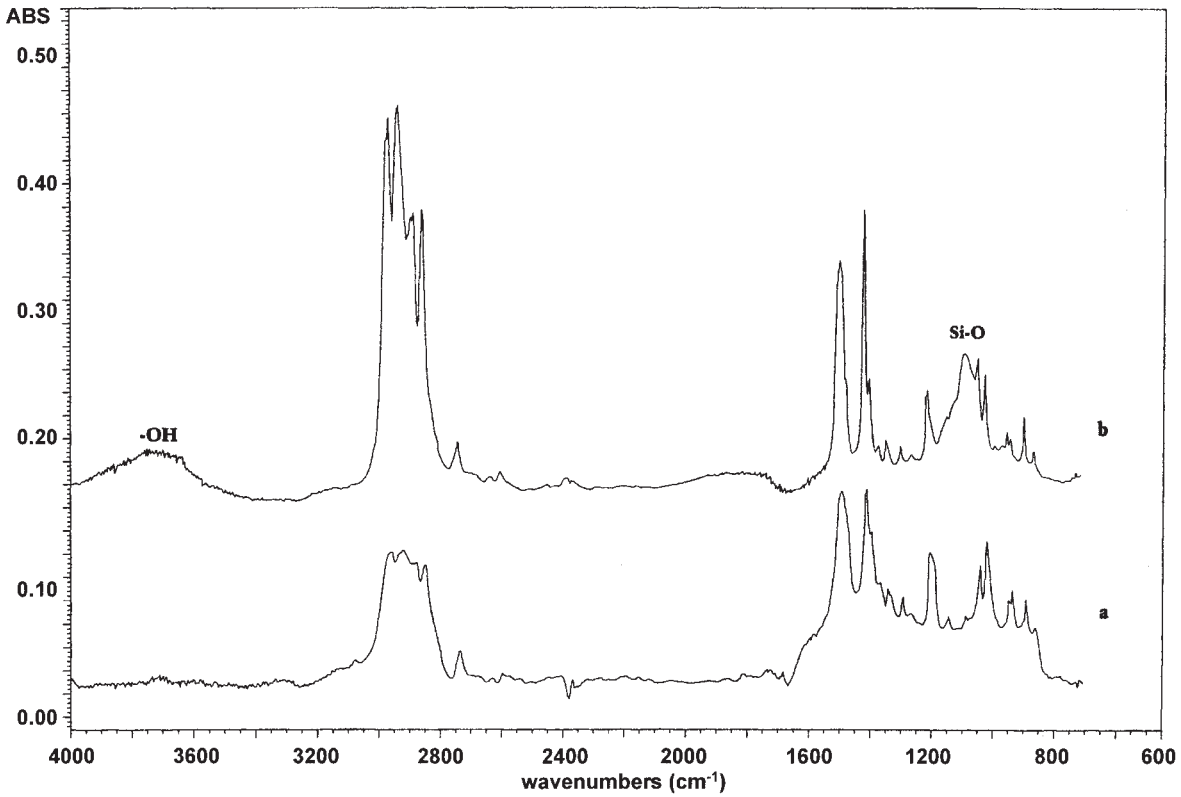

Figure 7 The FTIR spectrum of (a) PP; (b) PP-Mont nanocomposite.

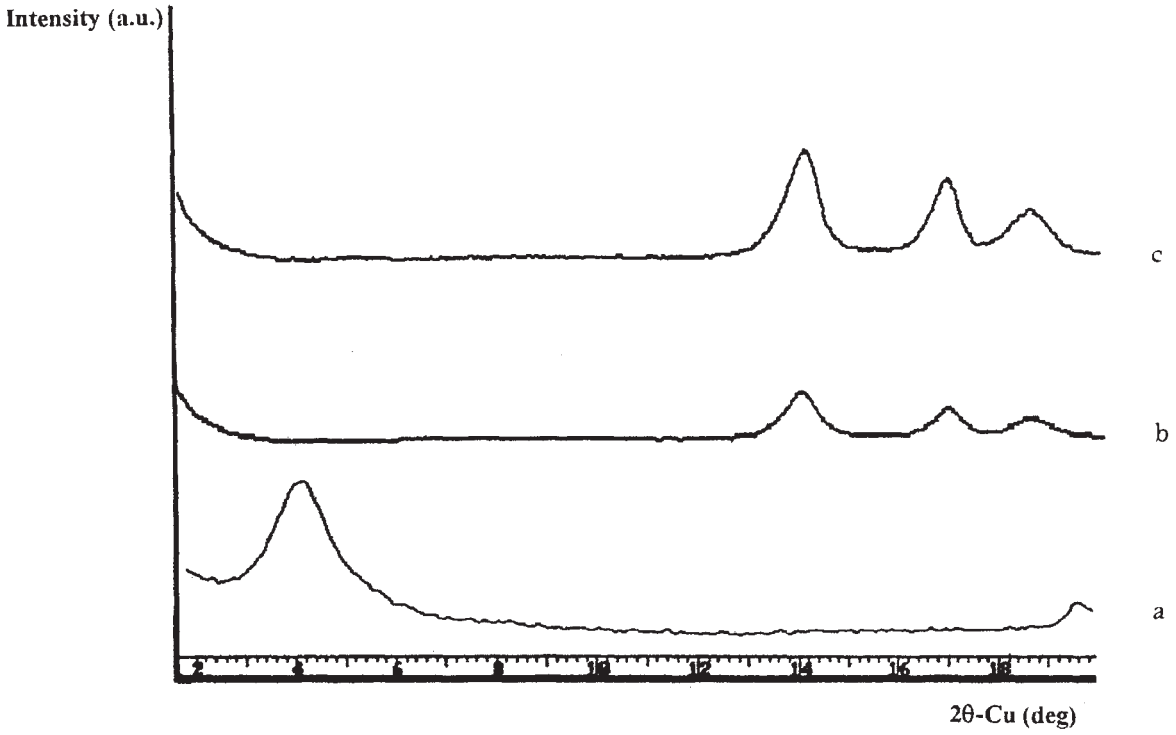

Figure 8 The XRD patterns of (a) O-Mont (prepared by SAC); (b) PP; (c) PP-Mont nanocomposite.

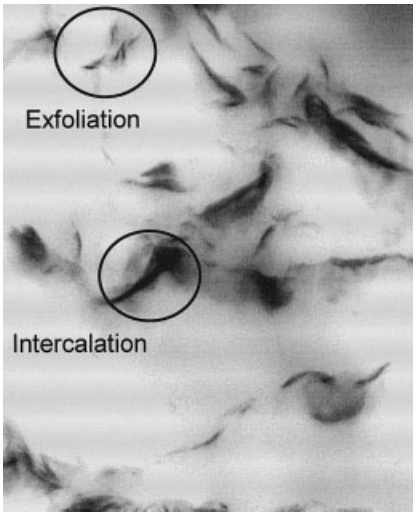

Figure 9 TEM photograph of PP-Mont nanocomposite.

Table II presents some results that pertain to PP-Mont nanocomposites generated by using *rac*-Et(Ind)$_2$ZrCl$_2$-supported catalysts. When O-Mont was added in the polymerization of propylene, both yield and activity decline rapidly because the number of activity centers fell when the catalyst was fixed on the montmorillonite, consistent with the observed low activity associated with coated catalytic particles.[31] The use of supported catalysts causes the yield and activity to increase with the reaction temperature and the concentration of the catalyst. However, the Mont contents (3–30 wt %) in the PP composites can be controlled by changing the reaction conditions.

The melt temperature and enthalpy of pure PP were 130.0°C and 67.3 J/g, respectively, at a reaction temperature of 40°C. The melt temperature (T_m) was closely related to the [mmmm] pentad value that is the stereoregularity of isotactic PP. Table II clearly indicates that the PP-Mont nanocomposite has more [mmmm] so that the PP-Mont nanocomposite has a higher T_m and ΔH than PP under the same reaction conditions. Meanwhile, the melt temperature and [mmmm] values of PP-Mont nanocomposites sharply decline as the reaction temperature rises. When the reaction temperature reaches 80°C, the melt temperature of the PP-Mont nanocomposite falls to about 50°C. The metallocene catalyst is less stereoselective and regioselective at higher temperatures, as has been frequently observed for other MAO-activated metallocene catalysts.[32]

The hardness can be calculated by the formula $HV = 0.102 \times F/d^2$ (where d is the diagonal length of the across the indentation). In this experiment, the force (F) was 9.87×10^{-2} N. Table II shows that the HV value of PP is 5.24 N/mm^2. Nevertheless, the PP-Mont nanocomposite has a larger HV value than pure PP. Additionally, the HV value increases with the Mont content. It demonstrated that the silicate sheets of Mont could provide the good hardness property in the composite.

The morphology of the PP and PP-Mont nanocomposite was elucidated by SEM. The shape of the pure PP particles resembles that of the *rac*-Et(Ind)$_2$ZrCl$_2$ catalyst, as depicted in Figure 10(a, b). The particle sizes are about 4–6 μm at a reaction temperature of 40°C but the PP particles fragment into smaller particles at higher reaction temperatures [Fig. 10(a, b)]. The shapes of PP-Mont nanocomposites differ completely from those of PP, as shown in Figure 10(c, d). The larger particles of PP-Mont particles are obtained by the *rac*-Et(Ind)$_2$ZrCl$_2$-supported catalyst and the diameters of the particles are estimated as being 10–30 μm. Larger particles increase the bulk density of the PP-Mont nanocomposite. However, the bulk density of PP-Mont nanocomposites clearly increases with the Mont content (Table II).

CONCLUSION

In this work, PP-Mont nanocomposites were successfully synthesized by *rac*-Et(Ind)$_2$ZrCl$_2$-supported catalysts on montmorillonite. The XRD and TEM show that the silicate layers of montmorillonite were ran-

TABLE II
Properties of PP and PP-Mont Nanocomposites by Using *rac*-Et(Ind)$_2$ZrCl$_2$ Catalyst[a]

No.	[Zr] (μmol)	Temp. (°C)	Yield (g)	Act[c] ($\times 10^{-6}$)	Mont cont. (wt%)	mmmm (%)	T_m (°C)	ΔH (J/g)	T_d (°C)	Density (g/cm^3)
P-1[b]	5	40	27.3	10.92	—	73.7	130.0	67.3	334.7	0.87
P-2[b]	5	80	17.3	6.92	—	66.8	73.3	26.0	405.0	0.85
PCH-1	30	40	2.4	0.08	12.6	77.1	134.9	88.2	257.8	0.94
PCH-2	40	40	2.5	0.06	11.9	83.7	134.3	78.6	260.6	0.92
PCH-3	50	20	1.1	0.02	28.6	88.5	139.7	63.3	239.1	—
PCH-4	50	40	3.2	0.06	9.4	87.3	134.3	87.1	255.9	0.90
PCH-5	50	80	8.1	0.16	3.7	73.6	87.0	33.6	263.4	0.88

[a] mont = 0.3 g, toluene = 100 ml, propylene pressure = 20 psi, reaction time = 1 h, [Al]/[Zr] = 100.
[b] Toluene = 100 ml, propylene pressure = 20 psi, reaction time = 30 min, [Al]/[Zr] = 1000.
[c] Act. = [g product]/[mol catalyst $\times$ h].

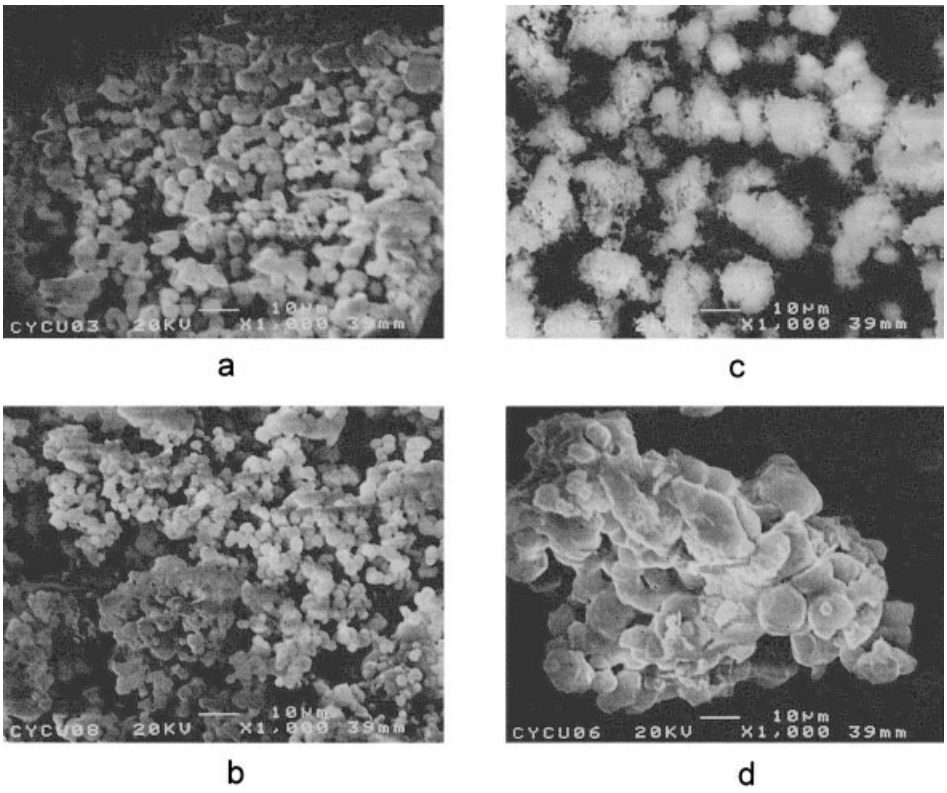

Figure 10 SEM photographs of PP at (a) 40°C (P-1); (b) 80°C (P-2); and PP-Mont nanocomposite at (c) 40°C (PCH-4); (d) 80°C (PCH-5).

domly dispersed in the PP matrix. The PP nanocomposites had a higher isotactic crystallinity, bulk density, Vicker hardness, melt temperature, and enthalpy than pure PP.

References

1. Usuk, A.; Fukushime, Y.; Fujimoto, M., Kojima, Y.; Kamigai, O. U.S. Pat. 4,889,885, 1989.
2. Usuki, A.; Koiwai, A.; Kojima, Y. J Appl Polym Sci 1995, 55, 119.
3. Vaia, R. A.; Jandt, K. D.; Kramer, E. J.; Giannelis, E. D. Macromolecules 1995, 28, 8080.
4. Sikka, M.; Cerini, L. N.; Ghosh, S. S.; Winey, K. I. J. Polym Sci, Polym Phys Ed 1996, 34, 1443.
5. Naoki, H.; Hirotaka, O.; Masaya K.; Arimistu, U. J Appl Polym Sci 1999, 74, 3359.
6. Kazuhisa, Y.; Arimitsu, U.; Akane, O.; Toshio K.; Osami, K. J. Polym Sci, Polym Chem Ed 1993, 31, 2493.
7. Lee, D. C.; Jiang, L. W. J Appl Polym Sci 1996, 61, 1117.
8. Guohua, C.; Kangde, Y.; Jingtia, Z. J Appl Polym Sci 1999, 73, 425.
9. Jiang, G. J.; Tsai, H. Y. Polym Prep 2000, 41, 621.
10. Usuki, A.; Kato, M.; Okada, A.; Kuranchi, T. J Appl Polym Sci 1997, 63, 137.
11. Kato, M.; Usuki A.; Okada, A. J Appl Polym Sci 1997, 66, 1781.
12. Kawasumi, M.; Hasegawa, N.; Kato, M.; Usuki A.; Okada, A. Macromolecules 1997, 30, 6333.
13. Hasegawa, N.; Kawasumi, M.; Kato M.; Okada, A. J Appl Polym Sci 1998, 67, 87.
14. Yermakov, Y. I.; Zakharov V. A.; Nesterov, G. A. in Catalytic Polymerization of Olefins; Kett T.; Kazuo S., Eds.; Studies in Surface Science and Catalysis; Elsevier: Amsterdam, 1986; p. 181.
15. Banks, R. L.; Cook, C. F. Catalyst Technology: Discovery to Commercialisation, Disproportionation of Propylene in Modern Aspect of Catalysis; Nauka: Novosibirsk, 1978; p. 149.
16. Bailey, D. C.; Langer, S. H. Chem Rev 1981, 81, 105.
17. Kaminsky, W. J Chem Soc, Dalton Trans 1998, 9, 1413.
18. Ewem, J. A. Sci Am 1997, 60.
19. Jiang, G. J.; Hwu, J. M.; Lai, K. J Polym Prep 1996, 37, 350.
20. Jiang, G. J.; Wang, T. Y. J Chin Chem Soc 1998, 45, 341.
21. Jiang, G. J.; Hwu, J. M. Polym Prep 1997, 38, 243.
22. Jiang, G. J.; Hwu, J. M. J Polym Sci, Polym Chem Ed 2000, 38, 1184.
23. Ribeiro, M. R.; Deffieux, A.; Portela, M. F. Ing Eng Chem Res 1997, 36, 1224.
24. Moroz, B. L.; Semikolenova, N. V.; Nosov, A. V.; Zakhoarov, V. A.; Nagy, S.; Oireilly, N. J. J Mol Catal, Chem 1998, 130, 121.
25. James, C. W. C.; Ben, M. G. J. Polym Sci, Polym Chem Ed 1993, 31, 1747.
26. Aria, H. T.; Uozumi, B. T.; Soga, K. Macromol Chem Phys 1997, 198, 229.
27. Quijada, R. A.; Rojas, R.; Narvaez, A.; Alzamoral, L.; Retuert J.; Rabagliati, F. M. Appl Catal 1998, 166, 207.
28. Tudor, J.; Willington, L.; O'Hare, D.; Royan, B. Chem Commun 1996, 17, 2031.
29. Green, K. R. The Montmorillonite Minerals in The Differential Thermal Investigation of Clay; Mineralogical Society: London, 1957.
30. Hwu, J. M.; Jiang, G. J.; Gao, Z. M.; Xei, W.; Pan, W. P. J Appl Polym Sci 2004, 101, 91.
31. Stephan, J.; Sebasstian, K.; Rolf, M. J Polym Sci, Polym Chem Ed 1997, 35, 1.
32. Rieger, K. Polym Bull 1994, 32, 41.